

A Novel Control Strategy for Grid Connected VSC with LCL Filters

Controlling the errors by using the vector controller

¹Ch.Dasu Babu, ²A.Arjuna Rao

²Associate Professor

Department of Electrical and Electronics Engineering

Abstract - This paper propose a novel control strategy for grid connected VSC with LCL filters by using Fuel cell and PV cell . The proposed control strategy is inherently capable of attenuating the resonance phenomenon of such systems. This is an advantage over the existing methods which require additional damping techniques. Moreover the proposed vector control strategy is able to fully decouple the direct (d) and quadrature (q) components of the current in a rotating reference frame. The design procedure comprises a constrained optimization-based loop shaping. It utilizes the multi-input multi-output (MIMO) nonparametric model of the system along with a high-order linearly parameterized MIMO controller to form an open-loop transfer function matrix. Minimizing the second norm of the error between the open-loop transfer function matrix and a desired one the coefficients of the controller are optimally determined. Conducting several reference tracking scenarios the performance of the proposed vector controller is evaluated both by means of time domain simulation studies in MATLAB/Simulink and experimental results.

Index Terms - Convex optimization damping distributed generation high-order controller LCL-filter loop shaping micro grid resonance vector control voltage-source converter (VSC)

I. INTRODUCTION

DUE TO THE rapid development of renewable-energy related technologies pulse width modulation (PWM) voltage-source converters (VSCs) are attracting significant interest and attention as the interfacing unit between such energy resources and the utility grid. Moreover VSCs are utilized in various other power-electronic-based applications e.g. power filters electric drives flexible AC transmission technologies high voltage DC transmission systems etc. In all of these applications the VSC is interfaced to the utility grid through either L-or LCL-filters. The filter is mainly responsible for attenuating the switching harmonics generated by the VSC. LCL-filters however are preferred due to their lower cost and superior harmonic attenuation capability compared to L-filters.

Regardless of their application grid-connected VSCs generally require a regulation scheme for controlling their current. In case of L-filter-based systems the VSC current is regulated by well-known vector control strategies. For the vector control of LCL-filter-based VSCs however very limited specifically tailored vector control strategies exist. The conventional approach in such cases is to neglect the capacitor dynamics. Therefore the vector controller is designed by considering the equivalent series connection of the LCLfilter inductors simplifying the control problem to that of a first-order system. As third-order systems however LCL-filters could potentially result in oscillatory and/or unstable dynamic behavior if the closed-loop system is not properly damped. Therefore a damping strategy must accompany the vector controller.

The damping of the LCL-filter resonance has been extensively investigated in the literature and various methods have been proposed which are mainly classified in two main categories: (1) Passive Damping (PD) and (2) Active Damping (AD). Passive damping is mainly based on adding resistive elements to the LCLfilter. The simplest PD method is the series connection of a resistor with the capacitor. PD methods are generally straightforward to implement and provide effective damping if the filter parameters are properly chosen. The damping losses however could noticeably decrease the system overall efficiency unless the switching and sampling frequencies are sufficiently high. Contrary to PD methods AD ones do not require additional passive elements and damp the system by modifying the structure of the vector control strategy. AD methods could themselves be categorized in two main classes: (1) multiloop and (2) filter-based. In the multiloop approach controlling more system state variables compared to conventional current vector regulation approaches the potential resonance modes are damped and the stability is guaranteed. Therefore in such methods more than one current loop is required which necessitates more sensors leading to higher overall system cost. In the filter-based approach no extra sensors are required as low-pass or notch filters are added to the output of the controller to damp the closed-loop system. In none of the aforementioned approaches however the axisdecoupling i.e. the decoupling between the direct (d) and quadrature (q) current axes is considered.

This paper proposes a vector control strategy for the LCLfilter-based grid-connected VSCs that has inherent damping capability and does not require extra damping strategies. Moreover the proposed vector control strategy is able to fully decouple the dq -axes of the current. The design procedure shapes the open-loop and closed-loop transfer function matrices of the LCL-filter-based system. This is in contrast with the conventional approaches that design the controller matrix assuming an L-filter-

based system. The proposed controller guarantees system stability and provides satisfactory and robust performance over a wide range of operating points.

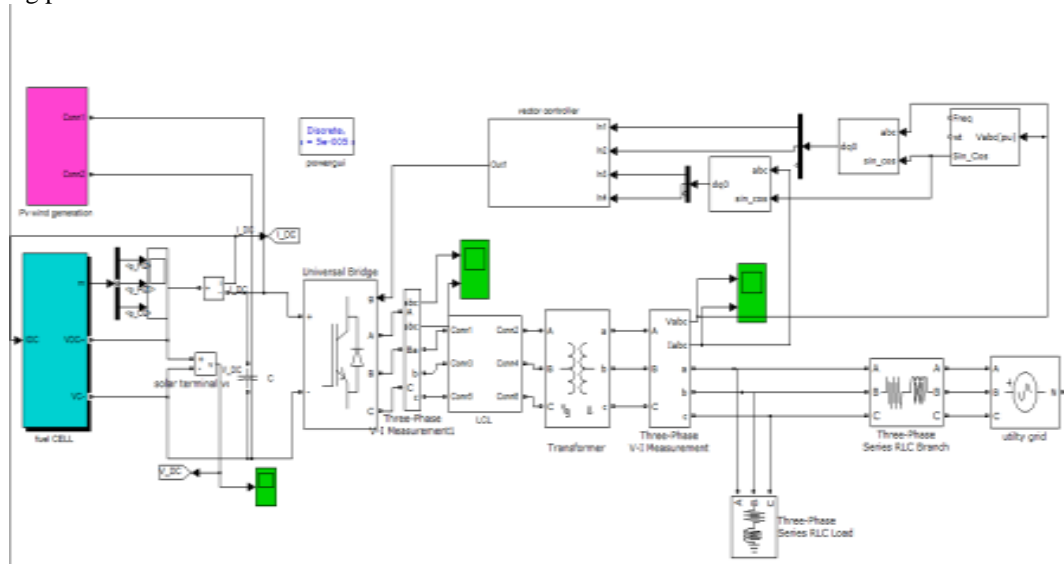


Fig. 1. Single-line diagram of the three-phase test system.

The elements of the controller matrix have an integrator similar to PI-controllers however they have more zeros which permit the controller matrix to compensate for the potentially unstable poles of the LCL-filter-based system. To determine the coefficients of the controller matrix a constrained optimization-based loop shaping method is adopted [25]. It uses the multi-input multi-output (MIMO) nonparametric model of the LCL-filter-based system along with a linearly parameterized high-order MIMO controller to form the open-loop transfer function matrix. Solving a constrained optimization problem the second norm of the error between the obtained open-loop transfer function matrix and a desired one is minimized and the coefficients of the assumed controller are optimally determined. The minimization problem guarantees the stability and desired dynamic performance of the closed-loop system. To ensure the axis-decoupling the off diagonal elements of the desired open-loop transfer function matrix are set to zero.

The rest of this paper is structured as follows. Section II describes the study system. Section III presents the proposed damping vector control strategy and details its design procedure. Based on simulation and experimental results the performance of the proposed vector controller is evaluated in Section IV. Section V concludes the paper.

II. STUDY SYSTEM DESCRIPTION

Fig. 1 shows the single-line diagram of the study system which comprises a three-phase VSC interfaced to the utility grid through an LCL-filter and a coupling transformer. The filter is composed of a grid-side inductor L_g a capacitor C and a VSC-side inductor L_c . The internal resistance of L_g and L_c are represented by R_g and R_c respectively. The VSC DC-side is fed by a continuous voltage source and therefore its dynamics are neglected in this paper. Table I presents the parameters of the study system of Fig. 1. According to the parameters of Table I the resonance frequency of the LCL-filter-based system is calculated as follows [26]:

$$f_{res} = \sqrt{((L_g+L_c)/L_gL_c.C)/2} = 1667\text{Hz} \quad (1)$$

TABLE 1 PARAMETERS OF THE STUDY SYSTEMS OF FIG.1

Quantity	Value	Comment
L_c	1.5 mH	LCL-filter Converter-side Inductor
R_c	0.1 Ω	Series Resistance of L_c
L_g	1.5 mH	LCL-filter Grid-side Inductor
R_g	0.1 Ω	Series Resistance of L_g
C	15 μF	LCL-filter Capacitor
S_{base}	0.8 kVA	VSC Rated Power
V_{dc}	120 V	DC Bus Voltage
v_g	60 V (peak)	Ph-Ph Nominal Voltage
f_{sw}	10 kHz	PWM Carrier Frequency
f_s	10 kHz	Sampling Frequency
$f_{s,id}$	5 kHz	Identification Sampling Frequency
f	50 Hz	System Nominal Frequency
f_{res}	1677 Hz	LCL-Filter Resonance Frequency

In the system of Fig. 1 for synchronization a phase-locked loop (PLL) is utilized which extracts the phase-angle of the grid voltage and forces its q-component to zero. Therefore to regulate the real and reactive power exchange a vector control strategy is adopted that controls the d- and q-components of the grid current which are proportional to the real and reactive power respectively. Feeding the errors between the dq-components of the grid current and their respective reference values to the controller the control signals i.e. the dq-components of the PWM block input signals v_{tdq} are then generated. The vector controller is also in charge of damping the system around its resonance frequency. All inputs/outputs of the proposed control system are illustrated in the respective block diagram of Fig. 1.

III. HIGH-ORDER DAMPING VECTOR CONTROL STRATEGY

In this section the design procedure of the damping vector control strategy for LCL-filter-based VSCs is detailed which is based on a constrained optimization-based loop shaping method [25]. It uses the MIMO nonparametric model of the system i.e. $G(j\omega)$ along with a linearly parameterized MIMO controller i.e. $K(z)$ to form an open-loop transfer function matrix i.e. $L(j\omega) = G(j\omega)K(j\omega) \forall \omega \in \mathbb{R}$.

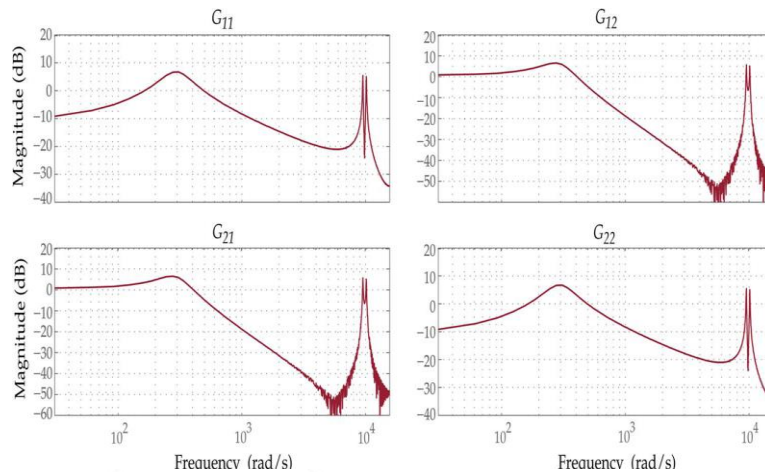


Fig. 2. Identified nonparametric model of the system of Fig. 1.

Based on the dynamic performance and the decoupling requirements a desired open-loop transfer function matrix i.e. $LD(s)$ is also formed and its diagonal and off-diagonal elements are determined. Minimizing the second norm of the error between the open-loop transfer function matrix and the desired one the coefficients of the controller are optimally determined. To ensure the stability and the required dynamic performance of the closed-loop system the minimization problem is subject to constraints. The design procedure is divided into three main steps:(1) the determination of the required non-parametric model, (2)the determination of the class of the controller, and (3) solving the optimization problem and finding the optimal coefficients of the controller. In the following, the steps are detailed.

A. Nonparametric Model

In order to design the damping vector control strategy the first step is to determine the nonparametric model of the system. The goal of the vector control strategy is to regulate the dq-components of the grid current i.e. $i_{g,dq}$ by providing the dq-components of the PWM input signals i.e. $v_{t,dq}$. Therefore the inputs of the to-be-controlled system are $v_{t,dq}$ while its outputs are $i_{g,dq}$. Thus the system transfer function matrix is

$$\begin{bmatrix} i_{g,d} \\ i_{g,q} \end{bmatrix} = \begin{bmatrix} G_{11} & G_{12} \\ G_{21} & G_{22} \end{bmatrix} \begin{bmatrix} v_{t,d} \\ v_{t,q} \end{bmatrix} \quad (2)$$

To achieve the nonparametric model of the system of Fig. 1 exciting $v_{t,d}$ with a stimulus signal e.g. pseudo random binary sequence (PRBS) [27] the frequency response of G_{11} and G_{21} could be identified as

$$G_{11}(j\omega) = F(i_{g,q}) / F(v_{t,d}) \text{ and } G_{21}(j\omega) = F(i_{g,q}) / F(v_{t,d}) \quad (3)$$

The same holds for obtaining G_{22} and G_{12} through the excitation of $v_{t,q}$. It must be noted that the identification sampling frequency i.e. $f_{s, id}$ could be different from the control sampling frequency i.e. f_s and in this paper $f_{s, id} = 5\text{kHz}$ which is compatible with the Shannon theorem.

Fig. 2 depicts the identified nonparametric model corresponding to the system of Fig. 1 whose parameters are set according to Table I. The identified nonparametric model confirms the resonance phenomenon at frequencies around the predicted resonance frequency of 1677 Hz. Therefore the controller matrix must be chosen and designed such that in the closed-loop system the gains at frequencies around the resonance frequency are well attenuated.

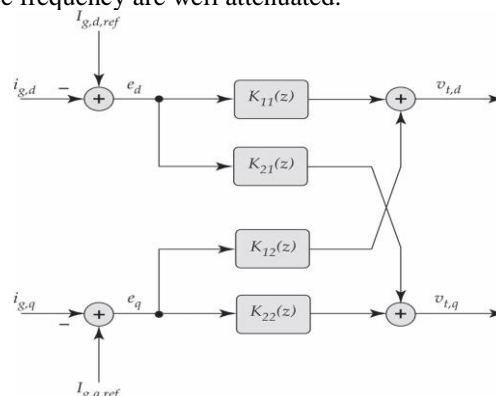


Fig. 3. Structural diagram of the controller.

B. Controller Class

The vector control strategy is responsible for regulating the *dq*-components of the grid current through manipulating the *dq*-components of VSC terminal voltage i.e. *vt dq*. Therefore to control such a system a 2×2 controller is required. A generic form of such a multivariable discrete-time controller in the *z*-domain is given by

$$\begin{bmatrix} vt, d \\ vt, q \end{bmatrix} = \begin{bmatrix} k11 & k12 \\ k21 & k22 \end{bmatrix} \begin{bmatrix} ed \\ eq \end{bmatrix} \quad (4)$$

where e_d and e_q are the current errors in the *d*- and *q*-axes respectively. The structural diagram of the controller is depicted in Fig. 3.

Conventional vector control strategies for L-filter-based VSCs utilize PI-controllers as the elements of the controller matrix. In such systems only one dominant pole exists in each axis which could be compensated by the zero of the utilized PI-controllers. In LCL-filter-based systems however this is no longer valid as more poles are introduced by the additional passive LC elements. Thus if PI-controllers are used for the vector control of LCL-filter-based all poles of the system may not be compensated and therefore damping strategies are required to attenuate the effects of the uncompensated poles. In this paper high-order controllers are utilized as the elements of the controller in order to compensate for all poles of the LCL-filter-based system such that no extra damping strategies are required. Thus each element of the controller matrix of (4) is a 5th-order controller in the *z*-domain. For example K_{11} is given by in which the vector ρ contains the controller matrix coefficients as follows:

$$K_{11}(z, \rho) = (\rho_1 + \rho_2 z^{-1} + \rho_3 z^{-2} + \rho_4 z^{-3} + \rho_5 z^{-4} + \rho_6 z^{-5}) / (1 - z^{-1}) \quad (5)$$

$$\rho = [\rho_1, \rho_2, \dots, \rho_6] \quad (6)$$

Therefore, the open-loop transfer function matrix of the LCLfilter- based system is given by

$$L(j\omega, \rho) = G(j\omega)K(j\omega, \rho) = \begin{bmatrix} L11 & L12 \\ L21 & L22 \end{bmatrix} \quad (7)$$

C. Optimization-Based Loop Shaping

The loop shaping of the open-loop transfer function matrix i.e. L is carried out by minimizing the square second norm of the error between the individual entries of L and a desired open-loop transfer function matrix $L_D(s)$. Consequently the control design procedure turns into an optimization problem as follows [25]:

$$\min \|L(\rho) - L_D\|^2 \quad (8)$$

The desired open-loop transfer function matrix L_D is chosen to meet the system requirements e.g. satisfactory dynamic response and reduced coupling between the outputs i.e. *ig d* and *ig q*. In this paper the desired open-loop transfer function is selected as

$$L_D(S) = \begin{bmatrix} \omega_c / s & 0 \\ 0 & \omega_c / s \end{bmatrix} \quad (9)$$

in which $\omega_c = 1200$ rad/s. Note that the bandwidth of the closed-loop system is manipulated by the choice of ω_c . In order to ensure the stability and also the dynamic performance of the to-be-designed controller the minimization problem is subject to several constraints. The reference proves that to shape the sensitivity function of the closedloop system the minimization problem must be subject to the following linear constraints:

$$|W_1(j\omega)[1 + L_{Dq}(j\omega, \rho)] - R_1 \{ [1 + L_{Dq}(-j\omega)] [1 + L_{qq}(j\omega, \rho)] \}| < 0 \quad \forall \omega \in \mathfrak{R} \quad \text{and } q=1,2.. \quad (10)$$

where $W_1(j\omega)$ is a weighting filter. In this paper, $W_1(j\omega) = 0.5$, which guarantees a gain margin of at least 2 and a phase margin of greater than 29° [28]. Moreover, to ensure the stability of the closed-loop system, the minimization problem must satisfy the generalized Nyquist stability criterion. Therefore, as proved in [25], the minimization problem must also satisfy the following constraints:

$$r_q(\omega, \rho) = \Re \{ [1 + L_{Dq}(-j\omega)] [1 + L_{qq}(j\omega, \rho)] \} / |1 + L_{Dq}(j\omega)| < 0 \quad \forall \omega \quad \text{and } q=1,2 \quad (11)$$

where $r_1(\omega, \rho)$ and $r_2(\omega, \rho)$ are defined as

$$r_1(\omega, \rho) = |L_{21}(j\omega, \rho)| \quad (12)$$

$$r_2(\omega, \rho) = |L_{12}(j\omega, \rho)| \quad (13)$$

The optimization problem of (8) constrained to (10) and (11) known as a semi infinite problem (SIP) includes infinite number of constraints and finite number of variables. A practical solution to this problem is to neglect the frequencies above a certain frequency i.e. ω_{max} for which the gains of the elements of the open-loop transfer function matrix are close to zero. In discrete-time systems the frequencies above the Nyquist frequency could be neglected. Moreover in order to have a finite number of frequency points the gridded frequency interval $[0 \omega_{max}]$

could be taken which contains finite frequency points. Therefore the SIP problem turns into a semi definite problem (SDP) and could be solved utilizing standard SDP-solvers e.g. SeDuMi. Choosing N linearly spaced frequencies within the range of $[0 \omega_{max}] \in \mathbb{R}$ the quadratic objective function is approximated by

$$\|L(\rho) - L_D\|^2 \approx \sum_{k=1}^N \|L(j\omega_k, \rho) - L_D(j\omega_k)\|_F^2 \quad (14)$$

Where $\| \cdot \|_F$ is the Frobenius norm [25]. Therefore, the following optimization problem is deduced:

$$\min_p \sum_{k=1}^N \|L(j\omega_k, \rho) - L_D(j\omega_k)\|_F \quad \text{subject to } |W_1(j\omega_k) [1 + L_{Dq}(j\omega_k)] - R_1 \{ [1 + L_{Dq}(-j\omega_k)] [1 + L_{qq}(j\omega_k, \rho)] \}| < 0 \quad \text{for } k = 1, \dots, N \text{ and } q = 1, 2$$

$$|r_q(\omega_k, \rho) - R_1 \{ [1 + L_{Dq}(-j\omega_k)] [1 + L_{qq}(j\omega_k, \rho)] \} / [1 + L_{Dq}(j\omega_k)]| < 0 \quad \text{for } k = 1, \dots, N, \text{ and } q = 1, 2.$$

Solving the minimization problem of (15) for the identified nonparametric model, the controller matrix is calculated in (16), matrix of the system of Fig. 1 for two vector controllers:

(1) the proposed damping vector controller and (2) the multivariable-PI vector controller.

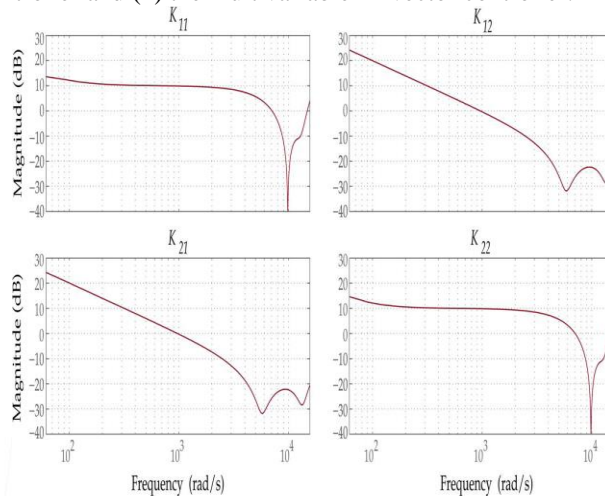


Fig. 4. Frequency response of the proposed damping vector controller.

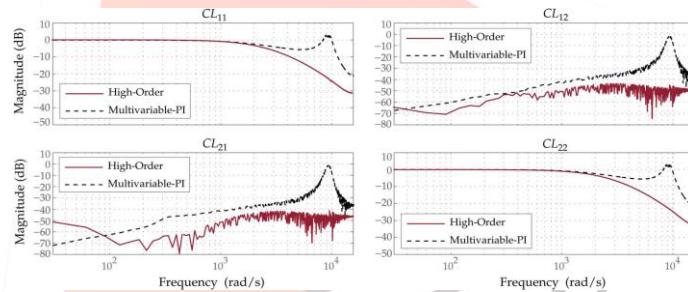


Fig. 5. Frequency response of the closed-loop transfer function

Shown at the bottom of this page. Obtaining the frequency response of the designed controller which is shown in Fig. 4 the frequency response of the open-loop transfer function matrix could be achieved as $L(j\omega) = G(j\omega)K(j\omega) \forall \omega \in \mathcal{R}$. Moreover the frequency response of the closed-loop system could be achieved as

$$K(z) = \begin{bmatrix} \frac{-2.760 + 7.112z^{-1} - 10.695z^{-2} + 9.996z^{-3} - 5.795z^{-4} + 2.116z^{-5}}{1 - z^{-1}} & \frac{-0.167 + 0.259z^{-1} - 0.240z^{-2} + 0.096z^{-3} + 0.004z^{-4} - 0.052z^{-5}}{1 - z^{-1}} \\ \frac{0.164 - 0.260z^{-1} + 0.255z^{-2} - 0.124z^{-3} + 0.022z^{-4} + 0.041z^{-5}}{1 - z^{-1}} & \frac{-2.768 + 7.153z^{-1} - 10.757z^{-2} + 10.045z^{-3} - 5.810z^{-4} + 2.112z^{-5}}{1 - z^{-1}} \end{bmatrix} \quad (16)$$

$$CL(j\omega) = \begin{bmatrix} CL_{11} & CL_{12} \\ CL_{21} & CL_{22} \end{bmatrix} = L(j\omega) / [1 + L(j\omega)] \quad \forall \omega \in \mathcal{R} \quad (17)$$

Fig. 5 depicts the frequency response of the closed-loop system of the LCL-filter-based system for two controllers:

- 1) a multivariable-PI vector control strategy for which no damping is used and
- 2) the proposed damping vector control strategy. It confirms that the proposed vector control strategy is capable of damping the closed-loop system around the resonance frequency while providing the same bandwidth as the multivariable-PI vector controller. Moreover the axis decoupling of the proposed vector control strategy as reflected in the very low gains of the off-diagonal elements of CL i.e. CL_{12} and CL_{21} is superior compared to the multivariable-PI case

D. Uncertainties in the System Parameters

The controller of (16) is designed for the system of Fig. 1 where the parameters are exactly set according to Table I. In order to obtain the required nonparametric model of such a system for the controller design identification is carried out in a simulation test bench. However the parameters of a dual experimental system could be different from those of the simulation-based case due to measurement errors in the LCLfilter values and/or grid impedance. Even if the identification is carried out directly on the experimental setup the aging phenomenon and/or identification errors could still lead to inconsistencies between the identified nonparametric model and the real one. Since designed for the nominal parameters of the system the controller of (16) may not

guarantee the stability of the system if the latter are substantially perturbed. However it must be noted that due to its extra zeros compared to conventional PI-controllers the high-order controller could still achieve a remarkable robustness margin with respect to variations in the system parameters.

In order to guarantee the robustness with respect to variations of the LCL-filter parameters and/or grid impedance the controller could be designed for a family of m nonparametric models corresponding to several values of the LCL-filters and/or grid impedance. Thus the stability of the system for the assumed family of models could be guaranteed. In such a case the design problem of (14) turns into the following:

$$\min_p \sum_{i=1}^m \sum_{K=1}^N \|L_1(j\omega_k, \rho) - LD(j\omega_k)\|_F \quad (18)$$

subject to

$$r_{i,q}(\omega_k, \rho) \left[|1 + L_{Dq}(j\omega_k)| - R \right] \left\{ |1 + L_{Dq}(-j\omega_k)| \left[|1 + L_{i,qq}(j\omega_k, \rho)| \right] \right\} < 0$$

for $k = 1, \dots, N$, $i = 1, \dots, m$, and $q = 1, 2$

$$|W1(j\omega_k) \left[|1 + L_{Dq}(j\omega_k)| - R \right] \left[|1 + L_{Dq}(-j\omega_k)| \left[|1 + L_{i,qq}(j\omega_k, \rho)| \right] \right| < 0$$

for $k = 1, \dots, N$, $i = 1, \dots, m$, and $q = 1, 2$.

In this paper for the sake of simplicity only one model corresponding to the system of Table I is utilized in the design which is proven to be adequate for demonstration purposes in terms of both accuracy and validity.

Fuel Cell: A fuel cell is a device that converts the chemical energy from a fuel into electricity through a chemical reaction with oxygen or another oxidizing agent. Hydrogen is the most common fuel, but hydrocarbons such as natural gas and alcohols like methanol are sometimes used. Fuel cells are different from batteries in that they require a constant source of fuel and oxygen/air to sustain the chemical reaction; however, fuel cells can produce electricity continuously for as long as these inputs are supplied.

PV Cell: PV cells are made of special materials called semiconductors and in this case, silicon. When a photon (a light particle) hits the panel, it has enough energy to knock an electron loose, allowing it to flow freely. The panel then has several electrical fields to force the electrons to move in a certain direction, creating a current which can be used to do work.

IV. PERFORMANCE EVALUATION

In this section the performance of the proposed damping vector control strategy for grid-connected VSCs with LCL filters is evaluated by means of simulation and experimental results.

A. Simulation Results

The simulation results of the proposed damping vector control strategy in the MATLAB/Simulink environment are reported in this section and are shown in Figs. 6–9. The LCL-filter-based grid-connected VSC of Fig. 1 is adopted whose parameters are set according to Table I. The damping vector control strategy regulates the dq -components of the grid current. The simulation studies are conducted to demonstrate the performance of the proposed controller under two scenarios: 1) reference tracking in the d -axis while the reference value of the q -axis is fixed and

2) Reference tracking in the q -axis while the reference value of the d -axis is fixed. Moreover the same reference tracking tests are repeated while the filter parameters are different from the ones used in the design procedure in order to evaluate the sensitivity of the proposed vector control strategy to the LCL-filter parameters variations

1) *Reference Tracking Tests: Reference Tracking in d-Axis:* The reference value of the q -axis is kept constant at -6 A while the reference value of the d -axis steps up from -2 A to 5 A at the time instant $t = 20$ ms

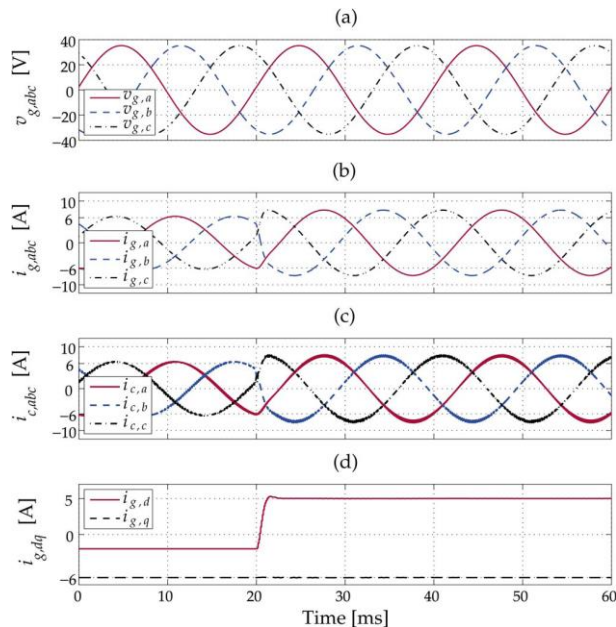


Fig. 6. Simulation response of the system of Fig. 1 to the reference change in the *d*-axis: (a) the three-phase grid voltage, (b) the three-phase grid current,(c) the three-phase converter current, and (d) the *d*- and *q*-components of the grid current.

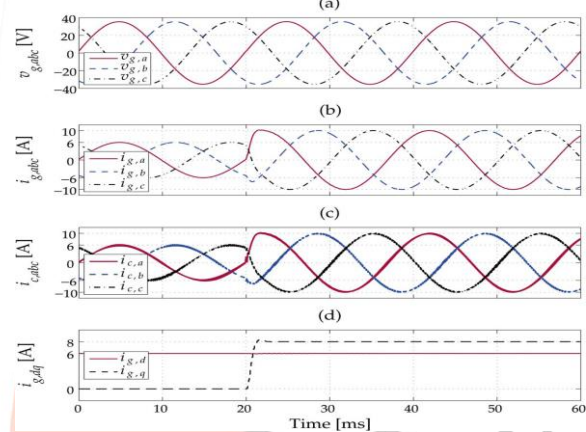


Fig. 7. Simulation response of the system of Fig. 1 to the reference change in the *q*-axis: (a) the three-phase grid voltage, (b) the three-phase grid current,(c) the three-phase converter current, and (d) the *d*- and *q*-components of the grid current implying a change in the active power flow as well. Fig. 6(a) depicts the three-phase grid voltage which remains unchanged during the reference tracking change. Fig. 6(b) and (c) show the three-phase converter and grid currents respectively. The *dq*-components of the grid current which are regulated by the high-order vector control strategy at their respective values are also shown in Fig. 6(d). The latter confirms that upon the step-change in the *d*-axis no resonance occurs in the system and the reference value is tracked in almost 1 ms. Moreover upon the step-change in the *d*-axis the *q*-axis remains unchanged proving the decoupling capability of the proposed controller

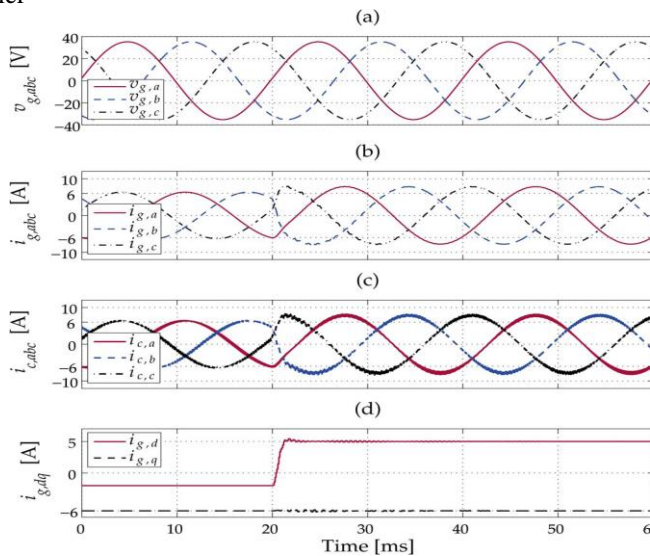


Fig. 8. Simulation response of the system of Fig. 1 to the reference change in the d -axis while the LCL-filter parameters contain uncertainties: (a) the three-phase load voltage, (b) the three-phase grid current, (c) the three-phase converter current, and (d) the d - and q -components of the grid current.

Reference Tracking in q -Axis: Another reference tracking test is carried out to evaluate the performance of the controller upon step-changes in the reference value of the q -axis while the reference value of the d -axis is fixed at 6 A. The reference value of the q -axis is stepped up from 0 to 8 A at the time instant $t = 20$ ms. Fig. 7(a)–(c) depict the three-phase grid voltage, grid current and converter current respectively. Prior and subsequent to the step-change the grid voltage remains unchanged while the grid and converter currents are changed by the controller. Fig. 7(d) shows the dq -components of the grid current which are regulated at their requested set-points. Upon the step-change in its reference value the q -component reaches its final value in almost 1 ms while the d -component is practically unaffected due to the decoupling effect of the controller. Moreover, the resonance is experienced neither upon the change of the reference signal nor in the steady-state operation.

2) Sensitivity to Filter Parameters:

In order to evaluate the sensitivity of the proposed controller to the variations in the LCL-filter parameters, two reference tracking tests similar to those of the previous section are conducted. The LCL-filter-based system of Fig. 1 is adopted in which the vector control block is the controller matrix of (16). The parameters of the system are also set according to Table I except for the LCL-filter whose parameters are $L_c = 1.5$ mH, $L_g = 0.9$ mH

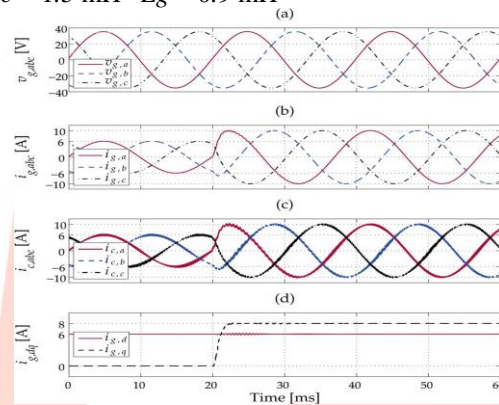


Fig. 9. Simulation response of the system of Fig. 1 to the reference change in the q -axis while the LCL-filter parameters contain uncertainties: (a) the three-phase grid voltage, (b) the three-phase grid current, (c) the three-phase converter current, and (d) the d - and q -components of the grid current and $C = 10$ μ F. Therefore, according to (1), the resonance frequency of this LCL-filter is 2113 Hz, which is significantly more than the resonance frequency of the LCL-filter for which the vector controller of (16) is designed.

In the first reference tracking test, the reference value of the q -axis is kept constant at -6 A and that of the d -axis steps up from -2 A to 5 A at the time instant $t = 20$ ms. The grid three-phase voltage is shown in Fig. 8(a) and the three-phase converter and grid currents are depicted in Fig. 8(b) and (c) respectively. The dq -components of the grid current are also shown in Fig. 8(d) which are accurately regulated at their reference values by the controller. Upon the step-change in the reference value of the d -axis, the d -component of the grid current tracks its reference in almost 1 ms. However, negligible resonance lasting for less than a cycle is visible on the dq -components of the grid current as well as on the converter and grid currents.

As the second reference tracking test, the d -axis reference value is set at 6 A while that of the q -axis changes from 0 to 8 A. The three-phase grid voltage, grid current, and converter current are depicted in Fig. 9(a)–(c) respectively. The dq -components of the grid current are also shown in Fig. 9(d). Upon the step-change in the q -axis reference signal, the controller regulates the q -axis of the grid current at its requested value in almost 1 ms while the d -axis is negligibly affected due to the resonance phenomenon for less than one cycle. The grid and converter currents also experience this negligible resonance for less than one cycle.

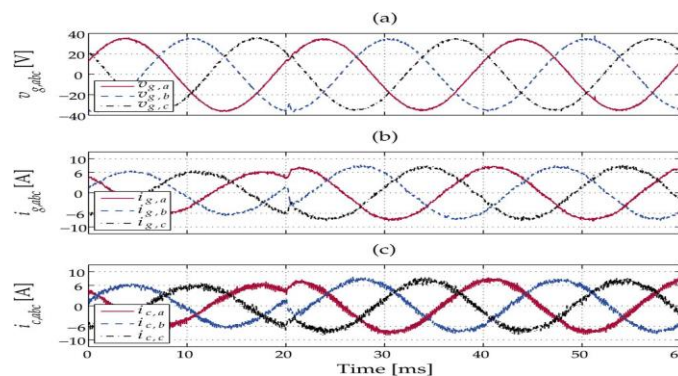


Fig. 10. Experimental results of the system of Fig. 1 to the reference change in the d -axis: (a) the three-phase grid voltage, (b) the three-phase grid current, and (c) the three-phase converter current.

The last two reference tracking tests confirm that the proposed vector controller is capable of regulating the dq -components and damps the system despite uncertainties in the LCL-filter parameters.

B. Experimental Results

In order to experimentally verify the findings two reference tracking tests similar to those of the simulation section are conducted. A laboratory prototype with the same layout as the study system of Fig. 1 is adopted whose parameters are set based on those given in Table I. The proposed high-order vector controller of (16) is implemented in a fully customized digital control platform based on a DSP/FPGA combination namely the *Boombbox* designed and developed in the Laboratory of Industrial Electronics at the EPFL [30].

Reference Tracking in d -Axis: The reference value of the q -axis is kept constant at -6 A while the reference value of the d -axis steps up from -2 A to 5 A at the time instant $t = 20$ ms. Fig. 10(a) depicts the three-phase grid voltage which is slightly affected upon the step-change in the current. The reason is that the internal impedance of the grid is not negligible in the experiment. Fig. 10(b) and (c) show the three-phase converter and grid currents respectively. Since a data logging scheme has not yet been implemented all measurements are captured by means of a digital oscilloscope and the dq -components of the grid current are not shown.

Reference Tracking in q -Axis: Another reference tracking test is carried out to experimentally evaluate the performance of the controller upon a step-change in the reference value of the q -axis while the reference value of the d -axis is fixed at 6 A. The reference value of the q -axis is stepped up from 0 to 8 A at the time instant $t = 20$ ms. Fig. 11(a)–(c) depict the three-phase grid voltage grid current and converter current respectively.

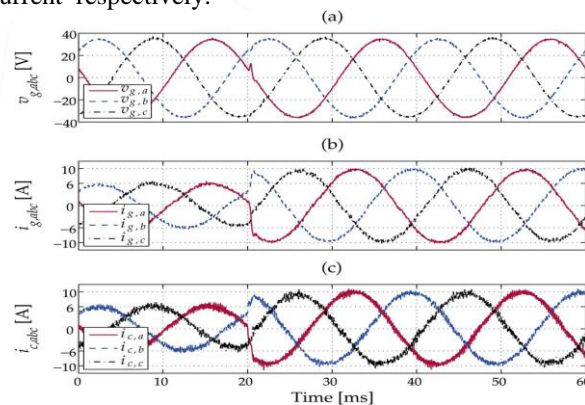


Fig. 11. Experimental results of the system of Fig. 1 to the reference change in the q -axis: (a) the three-phase grid voltage (b) the three-phase grid current and (c) the three-phase converter current. Subsequent to the step-change the grid voltage experiences minor transients due to its internal impedance.

In both aforementioned experimental tests the three-phase grid and converter currents follow the requested changes with zero steady-state error. Moreover the currents do not contain resonance frequency ripples which confirms the capability of the controller in terms of closed-loop system damping. In addition it can be observed that in all cases the experimental results are in very good agreement with the respective simulation results.

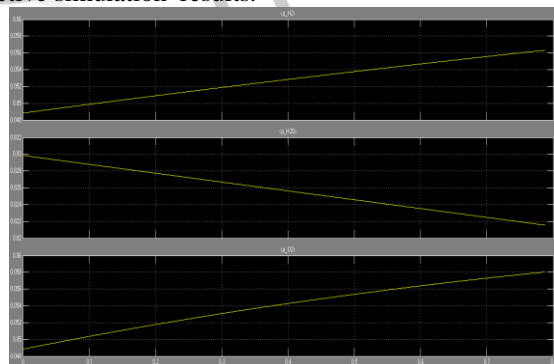


Fig 11: FUEL CELL CELL POWER WAVEFORM

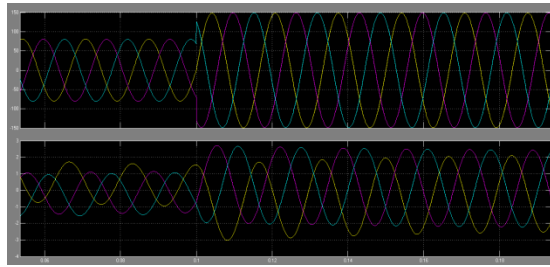


Fig 12: PV CELL CURRENT WAVEFORM

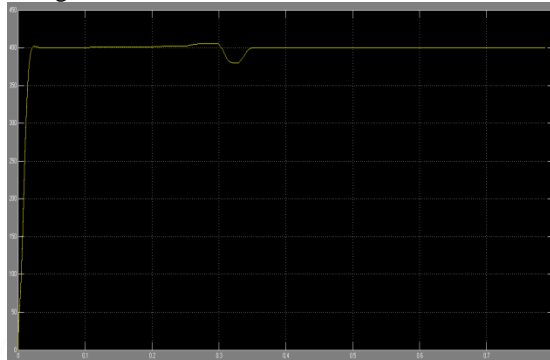


Fig 13: PV CELL VOLTAGE WAVEFORM

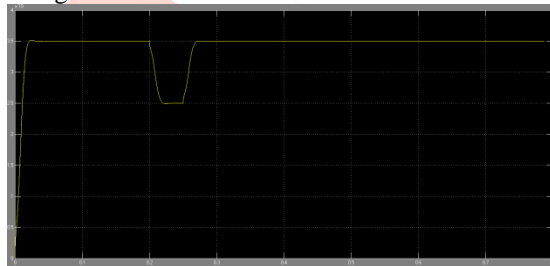


Fig 14: PV CELL POWER WAVEFORM

V. CONCLUSION

A novel control strategy for grid connected VSC with LCL filters by using Fuel cell and PV cell is proposed in this paper. To damp the resonance phenomenon of the LCL-filter a MIMO controller matrix is adopted whose elements are linearly parameterized high-order controllers with integrators. Contrary to the existing vector control schemes for VSCs with LCL-filters and PV cell the proposed approach does not require extra damping methods. Moreover the dynamic performance of the proposed approach is similar to the existing ones while its axis-decoupling capability is superior. The design procedure of the proposed controller is based on loop shaping and has three main steps: (1) attaining a nonparametric model of the system (2) determining the class of the to-be-designed controller and (3) solving a constrained convex optimization problem. The performance of the controller is evaluated for several reference tracking scenarios. Based on simulation and experimental results it is concluded that the proposed vector controller shows excellent dynamic performance in terms of reference tracking axis-decoupling and resonance attenuation upon step-changes in the set-points of the dq -components of current. Moreover despite uncertainties in the LCL-filter parameters the dynamic performance of the controller is acceptable.

REFERENCES

- [1] O. Senturk, L. Helle, S. Munk-Nielsen, P. Rodriguez, and R. Teodorescu, "Power capability investigation based on electrothermal models of presspack IGBT three-level NPC and ANPC VSCs for multimegawatt wind turbines," *IEEE Trans. Power Electron.*, vol. 27, no. 7, pp. 3195–3206, Jul. 2012.
- [2] B. Bahrani, A. Karimi, B. Rey, and A. Rufér, "Decoupled dq-current control of grid-tied voltage source converters using nonparametric models," *IEEE Trans. Ind. Electron.*, vol. 60, no. 4, pp. 1356–1366, Apr. 2013.
- [3] B. Bahrani, S. Kenzelmann, and A. Rufér, "Multivariable-PI-based dq current control of voltage source converters with superior axis decoupling capability," *IEEE Trans. Ind. Electron.*, vol. 58, no. 7, pp. 3016–3026, Jul. 2011.
- [4] B. Bahrani, A. Rufér, S. Kenzelmann, and L. Lopes, "Vector control of single-phase voltage-source converters based on fictive-axis emulation," *IEEE Trans. Ind. Appl.*, vol. 47, no. 2, pp. 831–840, Mar./Apr. 2011.
- [5] M. Liserre, R. Teodorescu, and F. Blaabjerg, "Stability of photovoltaic and wind turbine grid-connected inverters for a large set of grid impedance values," *IEEE Trans. Power Electron.*, vol. 21, no. 1, pp. 263–272, Jan. 2006.
- [6] P. Sun, C. Liu, J.-S. Lai, and C.-L. Chen, "Grid-tie control of cascade dualbuck inverter with wide-range power flow capability for renewable energy applications," *IEEE Trans. Power Electron.*, vol. 27, no. 4, pp. 1839–1849, Apr. 2012.
- [7] R. Teodorescu, M. Liserre, and P. Rodriguez, *Grid Converters for Photovoltaic and Wind Power Systems*. Hoboken, NJ, USA: Wiley, 2011.

- [8] H. Akagi and R. Kondo, "A transformerless hybrid active filter using a three-level Pulsewidth Modulation (PWM) converter for a medium-voltage motor drive," *IEEE Trans. Power Electron.*, vol. 25, no. 6, pp. 1365–1374, Jun. 2010.
- [9] V. Coroban-Schramel, I. Boldea, G.-D. Andreescu, and F. Blaabjerg, "Active-flux-based motion-sensorless vector control of biaxial excitation generator/motor for automobiles," *IEEE Trans. Ind. Appl.*, vol. 47, no. 2, pp. 812–819, Mar./Apr. 2011.
- [10] J. Chivite-Zabalza, M. Rodriguez Vidal, P. Izurza-Moreno, G. Calvo, and D. Madariaga, "A large power, low-switching-frequency voltage source converter for FACTS applications with low effects on the transmission line," *IEEE Trans. Power Electron.*, vol. 27, no. 12, pp. 4868–4879, Dec. 2012.
- [11] G. Kalcon, G. Adam, O. Anaya-Lara, S. Lo, and K. Uhlen, "Small-signal stability analysis of multi-terminal VSC-based DC transmission systems," *IEEE Trans. Power Syst.*, vol. 27, no. 4, pp. 1818–1830, Nov. 2012.
- [12] R. Teodorescu, F. Blaabjerg, M. Liserre, and P. Loh, "Proportional resonant controllers and filters for grid-connected voltage-source converters," *Proc. Inst. Elect. Eng.—Elect. Power Appl.*, vol. 153, no. 5, pp. 750–762, Sep. 2006.
- [13] V. Blasko and V. Kaura, "A novel control to actively damp resonance in input LC filter of a three-phase voltage source converter," *IEEE Trans. Ind. Appl.*, vol. 33, no. 2, pp. 542–550, Mar./Apr. 1997.
- [14] J. Dannehl, C. Wessels, and F. Fuchs, "Limitations of voltage-oriented PI current control of grid-connected PWM rectifiers with LCL filters," *IEEE Trans. Ind. Electron.*, vol. 56, no. 2, pp. 380–388, Feb. 2009.
- [15] R. Pea-Alzola, M. Liserre, F. Blaabjerg, R. Sebastian, J. Dannehl, and F. W. Fuchs, "Analysis of the passive damping losses in LCL-filter-based grid converters," *IEEE Trans. Power Electron.*, vol. 28, no. 6, pp. 2642–2646, Jun. 2013.
- [16] F. Blaabjerg, W. Wu, and T. Tang, "A new design method for the passive damped LCL- and LLCL-filter based single-phase grid-tied inverter," *IEEE Trans. Ind. Electron.*, vol. 60, no. 10, pp. 4339–4350, Oct. 2013.
- [17] M. Bierhoff and F. Fuchs, "Active damping for three-phase PWM rectifiers with high-order line-side filters," *IEEE Trans. Ind. Electron.*, vol. 56, no. 2, pp. 371–379, Feb. 2009.
- [18] A. Rockhill, M. Liserre, R. Teodorescu, and P. Rodriguez, "Grid-filter design for a multimewatt medium-voltage voltage-source inverter," *IEEE Trans. Ind. Electron.*, vol. 58, no. 4, pp. 1205–1217, Apr. 2011.
- [19] J. Dannehl, F. Fuchs, S. Hansen, and P. Thgersen, "Investigation of active damping approaches for pi-based current control of grid-connected pulse width modulation converters with LCL filters," *IEEE Trans. Ind. Appl.*, vol. 46, no. 4, pp. 1509–1517, Jul./Aug. 2010.
- [20] E. Wu and P. Lehn, "Digital current control of a voltage source converter with active damping of LCL resonance," *IEEE Trans. Power Electron.*, vol. 21, no. 5, pp. 1364–1373, Sep. 2006.
- [21] E. Twining and D. Holmes, "Grid current regulation of a three-phase voltage source inverter with an LCL input filter," *IEEE Trans. Power Electron.*, vol. 18, no. 3, pp. 888–895, May 2003.
- [22] P. C. Loh and D. Holmes, "Analysis of multiloop control strategies for LC/CL/LCL-filtered voltage-source and current-source inverters," *IEEE Trans. Ind. Appl.*, vol. 41, no. 2, pp. 644–654, Mar./Apr. 2005.
- [23] J. Dannehl, M. Liserre, and F. Fuchs, "Filter-based active damping of voltage source converters with LCL filter," *IEEE Trans. Ind. Electron.*, vol. 58, no. 8, pp. 3623–3633, Aug. 2011.
- [24] M. Liserre, A. Dell'Aquila, and F. Blaabjerg, "Genetic algorithm-based design of the active damping for an LCL-filter three-phase active rectifier," *IEEE Trans. Power Electron.*, vol. 19, no. 1, pp. 76–86, Jan. 2004.
- [25] G. Galdos, A. Karimi, and R. Longchamp, "H ∞ controller design for spectral MIMO models by convex optimization," *J. Process Contr.*, vol. 20, no. 10, pp. 1175–1182, Dec. 2010.
- [26] K. Jalili and S. Bernet, "Design of LCL filters of active-front-end two-level voltage-source converters," *IEEE Trans. Ind. Electron.*, vol. 56, no. 5, pp. 1674–1689, May 2009.
- [27] T. Söderström and P. Stoica, *System Identification*. Hempstead, U.K.: Prentice-Hall, 1989.
- [28] I. D. Landau, R. Lozano, M. M'Saad, and A. Karimi, *Adaptive Control, Algorithms, Analysis and Applications*. New York, NY, USA: Springer-Verlag, 2011.
- [29] J. F. Strum, "Using SeDuMi 1.02, a Matlab toolbox for optimization over symmetric cones," *Optim. Methods Softw.*, vol. 11, no. 1–4, pp. 625–653, Jan. 1999.
- [30] N. Cherix, S. Delalay, and A. Rufer, "Fail-safe modular control platform for power electronic applications in R&D environments," in *Proc. 15th Eur. Conf. Power Electron. Appl. (EPE-ECCE Europe)*, Lille, France, Sep. 2013.

Authors:



Ch. Dasu Babu was born in Visakhapatnam, Andhra Pradesh State in India, 1990. He received B.Tech degree from Gokul institute of technology and science Bobbili, Vizianagaram in 2011. He is pursuing M.Tech in Avanathi Institute of engineering and Technology, Bhogapuram, Vizianagaram.



A. Arjuna Rao was born in Visakhapatnam, Andhrapradesh State in India, 1977. He received B.Tech degree from Gayatri vidya parishad vizag, and his M.Tech degree from N.I.T., Rourkela and currently He pursuing Phd in Andhra University. He has eleven years of teaching experience and Currently He is Working as Associate Professor in EEE department of Avanathi Institute of engineering and technology, Visakhapatnam Andhra Pradesh State in India.

